5.1

Characterizing Annual Meteorological Modeling Performance for Visibility Improvement Strategy Modeling in the Southeastern US

Michael A. Abraczinskas*
North Carolina Division of Air Quality, Raleigh, NC

Donald T. Olerud, Jr and Aaron P. Sims
Baron Advanced Meteorological Systems, Raleigh, NC

1. INTRODUCTION

The Visibility Improvement State and Tribal Association of the Southeast (VISTAS) (http://www.vistas-sesarm.org/) is responsible for technical analyses and planning activities associated with the management of visibility and other regional air quality issues in the southeastern U.S. VISTAS analyses will support the states in their responsibility to develop, adopt, and implement their individual state air quality implementation plans for regional haze.

The objective of VISTAS atmospheric modeling is to evaluate emissions contributions to fine particulate pollution ($PM_{2.5}$) and visibility in the southeastern U.S. and to project how $PM_{2.5}$ and visibility will change in response to emissions changes. VISTAS has designed an extensive "one-atmosphere" modeling exercise which contains 3 main components: 1) meteorological modeling with MM5, 2) emissions modeling with SMOKE, and 3) chemical transport modeling with CMAQ. The meteorological modeling component is the primary focus of this paper.

Only a fraction of the comprehensive model evaluation is presented in the paper. Readers are strongly urged to visit the project web site for more complete analyses of the model performance and additional documentation at: (http://www.baronams.com/projects/VISTAS/)

2. APPROACH

In order to consider numerous areas in the southeastern U.S. simultaneously, a representative year is simulated. VISTAS chose to model the calendar year of 2002 using a 36-km grid for the national domain and a 12-km grid for the eastern U.S as shown in Figure 1. Prior to the annual simulation, a series of sensitivity tests were conducted to identify the optimal configuration for the southeastern U.S. Those findings are summarized in Olerud, (2004). This testing established the model configuration for the annual simulation.

* *Corresponding author address*: Michael A. Abraczinskas, North Carolina Division of Air Quality, 1641 Mail Service Center, Raleigh, NC 27699-1641; Michael.Abraczinskas@ncmail.net

The meteorological model used in this study is the PSU/NCAR Mesoscale Model (MM5 version 3.6.1+, Grell et al., 1994, MPP version), the same version of the code that was used in the sensitivity modeling. At the time the annual modeling began, the latest released version of the MM5 code was 3.6.2. Most of the v3.6.2 changes are included in the v3.6.1+ version of the code. The only modification not included involves the treatment of sea ice, a change likely to have negligible effect over the southeastern US. The v3.6.1+ code also includes an adapted version of EPA's MPP P-X code, an essential feature that does not readily port into later MM5 versions. The latest v3.6.2 MM5 preprocessors were employed.

The model configuration established through the aforementioned series of sensitivity tests was implemented for the annual run with the following physics options:

Soil: Pleim-Xiu land surface model
PBL: Asymmetric Convective Mixing
Radiation: Rapid Radiative Transfer Model
Cloud: Kain-Fritsch 2 cumulus parameterization
Microphysics: Reisner 1 (mixed phase)
Analysis nudging aloft:
36km: t (2.5E-4/s), q (1.0E-5/s), u and v (2.5E-4/s)
12km: t (1.0E-4/s), q (1.0E-5/s), u and v (1.0E-4/s)
Analysis nudging surface:
36km: u and v (2.5E-4/s), T and q not nudged
12km: u and v (1.0E-4/s), T and q not nudged
Observational nudging: Not used
Snow effects: Turned on via IFSNOW = 1
SST: EDAS 24-hr averaged skin temperatures
Vertical structure: 34 layers

Details on the various physics options listed above include Xiu and Pleim, (2001), Kain and Fritsch, (1993), Kain, (2002), Reisner et al, (1998), Mlawer *et al*, (1997).

The decision to use sea surface temperatures (SST's) derived from the EDAS skin temperatures was not an arbitrary one. At the time our modeling began, most of the other Regional Planning Organizations (RPO's) have decided to use NCEP SST's to avoid problems that might arise from applying skin temperatures as SST's. The 1996 annual modeling effort conducted by Olerud *et al* (2000) suffered from very high inland lake

temperatures as the MM5 system erroneously applied land skin temperatures to areas such as the Great Salt Lake. Fortunately the 3.6.2 version of the MM5 preprocessor INTERPF treats skin temperatures in a more appropriate manner, forcing a 24-hour average of skin temperatures if they are being used as a surrogate for SST's. The downside of using the NCEP SST fields is that they have a very coarse resolution of 2.5 x 2.5 degrees (~270 x 270 km). Alternatively the EDAS fields are available at 40-km resolution. Limited test runs were made using the each of the SST initialization options. Differences between the two approaches were clearly seen in the Gulf of Mexico. Overall, the results of the EDAS skin temperature test appeared to be the most reasonable.

Additional information on model set-up and execution can be found in the VISTAS Meteorological modeling protocol Olerud, (2004) at: http://www.baronams.com/projects/VISTAS/reports/VISTAS_TASK3a_draft.pdf

3. EVALUATION

The amount of data produced in this annual MM5 simulation is foreboding. One needs to consider a variety of primary and secondary meteorological variables, and often these variables need to be examined spatially, vertically, and temporally. Obviously we need to find a way to summarize the results, while concurrently allowing sufficient detail so that possibly important hourly/diurnal variations are not glossed out. To accomplish this we have divided the analyses into two main categories: Segment analyses, and monthly analyses.

3.1 Segment Analyses

The segment analyses examine the useable portion of each 5.5-day segment in considerable detail, focusing on surface data, aloft data, and statistical data. We examine surface data in 6-hourly spatial animations, with observations overlaid when applicable. This allows us to determine qualitatively if the model is replicating the observed spatial pattern, and also if model performance has a noticeable diurnal variation. These animations are available for every Regional Planning Organization (RPO) region (and sometimes sub-RPO region) as appropriate. Figure 2 shows the observing stations color-coded by RPO; the rectangular region plotted for each RPO includes all of its observing sites. The variables plotted as spatial animations include temperature, mixing ratio, wind vectors, cloud fraction, alternative cloud fraction, relative humidity, precipitation, and planetary boundary layer (PBL) height.

Time series of key meteorological variables at over 30 sites of interest, mostly in the VISTAS region are generated. We produce time series plots at both 36-km and 12-km (when applicable) resolutions, as well as figures with both resolutions plotted against the observations to allow for easy intrascale comparisons.

The final surface data product type is a "combination" plot, which is simply a spatial model field juxtaposed with the most appropriate observational image. These combination plots are produced once a day for visible satellite imagery/model clouds (18Z) and 24-h CPC accumulated precipitation/model precipitation (12Z), and twice a day (00Z, 12Z) for surface analysis/model pressure-winds-precipitation and infrared satellite imagery/model clouds.

The second segment analyses type is aloft products. These products include spatial analyses, sounding plots, and profiler plots. It is impractical to examine every one of the 34 model layers in detail, so we have decided to focus on three levels aloft for our spatial analyses. The three sigma-layers are layer 9 (~500m), layer 17 (~1600m), and later 22 (~3400m). This allows us to visualize model performance 1) in the PBL, 2) near the top of/just above the PBL, and 3) in the free troposphere. These aloft spatial plots are very similar in nature to the corresponding plots produced at the surface, though plots for only temperature, mixing ratio, and winds are produced at a 12-hr temporal resolution.

Upper air soundings were produced to examine the ability of the model to capture vertical variations. These plots are made for every rawinsonde site in the VISTAS region, plus a sampling of sites across the country. Full surface-to-100 mb soundings were produced, along with plots examining only the lower portions of the atmosphere (surface-to-500 mb).

Figure 3 shows an example of the final aloft evaluation product, the profiler plot. These plots compare model predicted winds with profiler-derived winds over the lowest 2500 meters of the atmosphere. Profilers yield results at a much finer vertical and temporal resolution than do standard rawinsondes. The profiler data are not used to nudge MM5, and in fact cannot effectively be used in that capacity without additional quality control to remove/correct erroneous data.

Each modeling segment also contains a variety of statistical products. Table 1 shows an example of a surface summary statistical table (all hours) for the 12-km VISTAS region for a modeling segment. Most of the variable names, while cryptic, are unambiguous and require no further explanation. We should note that CLD refers to the MCIP2.1 variable "CFRAC", while CLD2 refers to the maximum of MCIP2.1 variables "CFRACH", "CFRACM", and "CFRACL". The latter variable precisely matches the manner in which the observational cloud coverage is calculated, and is generally preferred for the purpose of

meteorological analysis. We should also note that "bias" for wind direction should be ignored in favor of "dbias", the appropriate bias calculation for a non-continuous function line wind direction. Also, "jtot" simply represents the number of model/obs pairs that go into the statistical calculations. While the sample table includes all valid hours within the modeling segment, we also produce tables that include only the 00-11Z hours (to highlight nighttime performance) and 12-23Z hours (to highlight daytime performance). These statistical tables are available for all applicable RPO's and RPO aggregates (i.e. US, Full). Each modeling segment also contains a full suite of statistical time series plots, both at the surface and aloft.

3.2 Monthly Analyses

Data was aggregated into monthly periods to assess model performance in a more complete manner. However, a couple of points about our statistical processing methodology should be made. The first involves the manner in which elevation discrepancies between the observations and the model are treated. We have rather arbitrarily decided that if the elevation of an observational site is more than 500 meters different than the model elevation, then that observing site is deemed unrepresentative and is not included in the statistical analyses. Mount Washington, NH (KMWN) is such a station. Even with automated quality control of the observational data, KMWN still occasionally stands out as an unrepresentative site in the Mid-Atlantic NorthEast-Visibility Union (MANE-VU) spatial analyses plots of temperature and especially winds. If the elevation of a site is within 500 m of the model elevation, we include it in our processing, but not without attempting to account for biases that surely arise solely due to the elevation difference. There is no easy way to deal with these elevation differences, but to ignore their effect is probably worse than crudely accounting for them. Our methodology is to apply a standard atmosphere adjustment (6.5C/km) to the elevation differences. Figure 4 shows the magnitude of these adjustments that were subtracted from the model temperatures before comparing with the observations. Note that for much of the western U.S., except along the coastline, the majority of sites are adjusted by a factor larger than the "benchmark" standard for temperature bias. This elevation effect is rather small for most of the rest of the country.

Another factor to consider in statistically evaluating model performance is the presence of observed calm winds. A calm wind report does not mean that the wind speed is identically 0.0 kts; rather, it means that the true wind speed is less than the instrument threshold. The lowest non-zero wind speed reported is 3 kts. The actual wind speed could thus be 0, 1, or 2 kts. Since the model will never completely "calm out", this instrument threshold issue introduces a positive wind speed bias to a perfect model simulation. This can play a significant role in the southeastern US, especially at night and in the summer, when stagnant high-pressure systems routinely cause numerous calms to be reported. In an attempt to quantify the magnitude of this effect, we have introduced two additional wind speed metrics to our summary table. The variable "WSPD-no_calms" quantifies wind speed statistics when all calm reports are thrown out. This approach, however, introduces a negative speed bias, since the < 3 kt winds are removed only in the observations. Probably a less biased approach is to simply assign a 1.5 kt wind speed to all calm reports. The variable "WSPD-min_calm" quantifies the result when that approach is applied.

Monthly summary statistical tables were produced for all applicable RPO's and for both grids. Since the precipitation statistics are commiserate with only two grid/scale combinations – 12-km Full and 36-km US – those are the only tables that include said information. An example statistical overview table is shown in Table 2. This table includes January 2002 12-km full domain statistics. Recall the meteorological statistical benchmarks reported by Emery (2001):

Wind speed: RSME ≤ 2 m/s, Bias ≤ +/- 0.5 m/s, IA ≥ 0.6

Wind direction: Gross Error ≤ 30 deg, Bias ≤ +/- 10 deg.

Temperature: Gross Error ≤ 2 K, Bias ≤ +/- 0.5 K, IA ≥ 0.8

Humidity: Gross Error ≤ 2 g/kg, Bias ≤ +/- 1 g/kg, IA ≥ 0.6

Note that the benchmarks were developed not to provide a pass/fail standard to which all modeling results should be held, but rather to put the results into an historical context. We also note that only a few of the numerous statistical measures that we show are actually included in the above benchmarks. If a particular relevant metric fails to fall within the benchmarks, that metric will be colored red for easy identification (as is the case for 1.5 m temperature bias and error in Table 2). Additionally, layer 1 temperature and wind speed are included in the tables, but only to put the more relevant 1.5-m temperature and 10-m wind speed statistics in context. Therefore, those metrics will not be compared to the benchmarks via color-coding.

4. RESULTS

Now that we have a general overview of the suite of model evaluation products available, let's turn our attention to how specific statistical quantities vary throughout the year and from grid to grid, examining

the possible causes of model performance weaknesses. To do this we will focus on the VISTAS region, cleanly comparing results at 36-km and 12-km resolutions. Figure 5 shows how monthly temperature biases vary throughout 2002. Note that the biases are generally small, never exceeding +/- 0.8C. Nonetheless the model shows a clear predilection towards being too cold in the winter months, and the problem is exacerbated at 12-km. Presumably the increased temperature nudging strength aloft (2.5 E-4/s vs. 1.0 E-4/s) enables the coarser 36-km grid to be slightly less biased. Model biases for the May-August period are practically 0.0 at both resolutions.

To examine the temperature biases in greater detail, consider the day (12Z-23Z) and night (00Z-11Z) bias traces for the 12-km grid in Figure 6. Clearly model performance for the daytime period is the primary reason for the wintertime cold bias. The daytime cold bias is persistent from month to month, but in the summer the model is only relatively weakly biased. The nighttime trace reveals that over the entire year the model is unbiased, being slightly low biased in the winter and slightly warm biased in the summer. There could be at least four physical mechanisms that could lead to a daytime cold bias: 1) Too cold soil initial conditions, 2) Too moist soil initial conditions, 3) Too many daytime clouds, and 4) Poor treatment of snow related processes. In general, the model temperature performance appears to be line with what we expect given the state of the art in MM5 applications.

To complete our statistical analyses of temperature, we have included "Bakergrams" in Figures 7 and 8 for the 12-km VISTAS region. Figure 7 shows the temperature bias in the Annual Bakergram. These images place daily statistics into a tile plot in a calendar-like layout. In this way we can effectively summarize performance for the entire year in one plot. Note how small the biases are in the summer, while the wintertime cold biases are easily seen. Figure 8 shows the temperature bias for January in a Monthly Bakergram. These plots display hourly biases in a tile plot format, with the day of the month increasing from left to right, and the UTC hour of the day increasing from top to bottom. Again note the cold bias is generally during the daylight hours.

Figure 9 shows the mixing ratio bias trace for 2002 for both model resolutions for the VISTAS region. The model exhibits a slight positive bias in January, especially at 36-km resolution. Considering that the average observed mixing ratio in January is on the order of 4 g/kg, this bias is more significant than an equivalent bias in July, when average observed mixing ratios are on the order of 15 g/kg. Might this positive moisture bias be the root cause of the temperature cold bias? Probably not, since the cold bias was larger in the 12-km grid, not the 36-km grid where the moisture bias is more significant.

Another striking observation about the mixing ratio bias traces is the low biases noted in the fall months, shown well in the seasonal plots in Figure 10. These values easily fall within the benchmark expectation of +/- 1.0 g/kg, but it is curious that the model shows that signature. Figure 11 shows the model is systemically dry-biased during the afternoon for non-winter months. Usually one associates such a feature with too much mixing (or too efficient mixing) in the model, thus bringing dry air from aloft to the surface. For most of the year the model is slightly moist biased at night, but in the fall the night shows a slight dry bias. The combination leads to the overall dry bias noted for that season. Figure 12 displays the site-specific moisture biases for September over the 12-km grid. Virginia and western North Carolina show the largest dry bias, while many areas (eastern NC, northern FL, MI) show a moist bias. Such spatial discrepancies in model performance over small areas suggest that either the model is failing to capture smaller-scale variations properly, or that the model is introducing smaller-scale variations where none exist. One of the striking differences between eastern North Carolina (moist bias) and western North Carolina (dry bias) is the soil types prevalent in those areas. Perhaps there are issues with the soil moisture/temperature initializations that lead to the performance differences over small areas? Figure 13 shows the September "Bakergram" for moisture bias over the 12-km VISTAS region. Recall that the model is run in 5-day segments such that every fifth day at 13Z results from a new segment are introduced. The first new segment in September starts on the 3rd. Moisture biases tend to be significantly worse at the beginning of a segment than they are at the end of a segment, indicating that there does indeed seem to be soil initialization issues that are affecting the model.

Wind speed performance was analyzed, starting with the standard "include-all-calms-as-zero" approach. Figure 14 shows that the model is positively biased with regard to wind speed for all months and for both grids. The bias is especially acute at 12-km resolution, presumably due to the weaker nudging applied to the winds at that scale. The greatest bias occurs in November, while the smallest bias occurs in March. Both are surprising results considering that summer and winter are the meteorological extremes. When we consider only non-zero wind speed observations, as shown in Figure 15, the resultant biases are practically non-existent at 12-km, while a slight low bias is evidenced at 36-km.

Let us now consider wind direction performance. Figure 16 shows the monthly wind direction errors over the VISTAS region for both model domains. The performance of the two grids is very similar, and surprisingly enough the 12-km grid has a slightly lower error. The increased nudging strength at 36-km might have been expected to yield

a lower direction error. We know that all wind direction errors do not have the same effect of air quality modeling. A 90 degree direction error at light winds speeds might have a less deleterious effect than a 40 degree error at moderate wind speeds. A better way of treating wind direction discrepancies between the model and the observations is to calculate the magnitude of the error wind vector. This approach properly treats winds as vectors and allows us to quantify the combined effect of speed and direction errors. Figure 17 shows the resultant plot. As a rule the two grids track very similarly, with the 36-km domain yielding slightly superior results, undoubtedly due to the presence of stronger nudging. Also note how the result for November does not stick out as an outlier, even though wind speed performance exhibited its highest bias during that month.

The alternative cloud fraction variable defined in this exercise "CLD2" is deemed more meteorologically consistent with the cloud observations than is the MCIP-derived variable "CLD". We will focus our attention there. Figure 18 shows a strong seasonal variation to cloud bias. For most of the year clouds are relatively unbiased. However, through the summer months a noticeable positive bias appears, especially at 12-km. Figure 19 shows most of the bias occurs at night. It is difficult to know if this nighttime bias is indeed real, since cloud observations at night might not be as accurate as they are during the daytime. An analysis of the average observed cloud coverage reveal a distinct diurnal variation in that cloud coverage is greatest in the afternoon and smallest in the late overnight periods. Another evident cycle occurs at the synoptic scale and can be seen on an approximately 10-day time scale. The model does a nice job replicating the synoptic scale variations, but the diurnal variations are completely out of phase. Since the nocturnal bias is more significant at 12-km than it is at 36-km, one must consider the possibility that the internal cloud parameterizations need to be adjusted to run as successfully at finer scale resolutions.

During the summary analysis of precipitation, monthly observation/model accumulated precipitation plots for the 12-km and 36-km grids were considered. For most of the year the model does a nice job in replicating the observed precipitation field. However, the model appears to noticeably overestimate the amount of precipitation in the summer months, especially July (Figure 20). Nonetheless, in the fall, the model underestimates precipitation amounts, coinciding with the dry bias noted in the mixing ratio statistics.

In examining the notable summertime precipitation accumulation bias, two scenarios were considered. One is the model generating spurious convection (raining too frequently). The second is the model generating too much rainfall (overestimating intensity) while correctly predicting the frequency. The first scenario is of most concern from an air quality modeling perspective, since the presence/absence of rain affects pollution concentrations more than predicting 2 inches of rain when only 1 inch actually occurred. An analysis of precipitation statistics for different threshold amounts was completed. Precipitation bias scores at the 0.01 and 0.05 inch thresholds are near 1.0 (i.e. unbiased), while bias scores at the 0.25 and 0.50 inch thresholds are significantly higher. These statistics indicate that the model suffers from the more benign weakness mentioned above, namely overestimating the predicted amount of precipitation when it actually occurs.

5. DISCUSSION

Model performance for the 12-month simulation in the southeastern U.S. is deemed adequate for visibility modeling. By and large, performance traits evident in the sensitivity modeling are seen in the annual simulation as well. Some general conclusions include:

1. Synoptic features were routinely accurately predicted, and the model showed considerable skill in replicating the state variables. Most of the time the model statistics easily fell within the expected "benchmarks".

2. The model shows evidence of being adversely affected by poor soil initialization at times. This is particularly evident for September and November, and it might cause the autumnal dry bias evidenced both in the mixing ratio statistics and also in the precipitation statistics. At the time of our modeling, the P-X LSM only allowed three soil initialization options: 1) Table look-up, 2) EDAS, and 3) interppx. Sensitivity testing showed that interppx can produce more severe cold biases, so we chose the EDAS option. Unfortunately that option initializes soil moisture from a layer 100-200 cm deep, whereas the P-X LSM extends downward only 100 cm. In the future improved model performance might be attained by more wisely initializing soil moisture.

3. The model is noticeably cold biased in the winter months. This was expected based on our sensitivity modeling, and it appears to be related to the manner in which soil temperatures are initialized.

4. The summertime diurnal cloud cycle appears to be out of phase with the observed cycle. The model maximizes cloud coverage at night and minimizes cloud coverage in the afternoon, while the observations indicate that the exact opposite should occur.

5. The model noticeably overestimates the amount of summertime precipitation, but not the spatial coverage of measurable precipitation.

6. While no modeling is perfect, the results of this effort should produce credible inputs for subsequent air quality modeling.

6. ACKNOWLEDGEMENTS

Atmospheric data were provided by the Data Support Section of the Scientific Computing Division at the National Center for Atmospheric Research. NCAR is supported by grants from the National Science Foundation. Original sources of the datasets ds353.4, ds464.0, and ds609.2 were provided to NCAR by the National Center for Environmental Prediction. The original source of dataset ds472.0 was provided to NCAR by the Techniques Development Laboratory.

Profiler data obtained from the NOAA Profiler Network were provided by Forecast Systems Lab. Daily US .25x.25 gridded precipitation observations were provided by the Climate Prediction Center. Visible and Infrared satellite imagery were obtained from the National Climatic Data Center's historical GOES browse server. Surface analysis maps were obtained from Unisys website, weather.unisys.com; the data on this site are provided from the National Weather Service via the NOAAPORT satellite data service.

Specific sites of surface station data for time-series plots were obtained from the National Park Service courtesy of NPS Air. These data are part of the Interagency Monitoring of Protected Visual Environments (IMPROVE) monitoring sites. Additional surface data from the SouthEastern Aerosol Research and Characterization Study experiment (SEARCH) were obtained from Atmospheric Research and Analysis, Inc. Other surface data were provided courtesy of SCDHEC and NCDAQ.

The authors would like to acknowledge MCNC Enterprise Grid Services for the use of their computation resources. We would like to thank Kirk Baker of LADCO for his initial development of the Mosaic summary plots (Bakergrams). We also would like to acknowledge Nick Witcraft of NCDAQ for the generation and use of most of the excel plots.

REFERENCES

Emery, C., E. Tai, and G. Yarwood, 2001. "Enhanced Meteorological Modeling and Performance Evaluation for Two Texas Episodes", report to the Texas Natural Resources Conservation Commission, prepared by ENVIRON, International Corp, Novato, CA.

Grell, G. A., J. Dudhia, and D. R. Stauffer, 1994: A description of the fifth-generation Penn State/NCAR Mesoscale Model (MM5). NCAR Tech. Note, NCAR/TN-398+STR, 122 pp.

Kain, J. S. and J. M. Fritsch, 1993: Convective parameterization for mesoscale models: The Kain-Fritsch scheme, *The Representation of Cumulus Convection in Mesoscale Models,* K. A. Emanuel and D. J. Raymond, Eds., American Meteorological Society, Boston, 246 pp.

Kain, John S., 2002: The Kain-Fristch convective parameterization: An update. To be submitted to J. of Appl.Meteoro.

Mlawer, E. J., S. J. Taubman, P. D. Brown, M. J. Iacono, and S. A. Clough, 1997: Radiative transfer for inhomogeneous atmospheres: RRTM, a validated correlated-k model for the longwave. J. Geophys. Res., 102(D14), 16,663-16,682.

Olerud, D. K. Alapaty, and N. Wheeler, 2000: Meteorological Modeling of 1996 for the United States with MM5. MCNC – Environmental Programs, Research Triangle Park, NC. Final report submitted to OAPQS, US EPA.

Olerud, D. and A. Sims, 2004: Protocol for Annual MM5 Sensitivity Modeling in Support of VISTAS (Visibility Improvement - State and Tribal Association)] VISTAS Task 3a deliverable. Available from Mike Abraczinskas, Meteorologist, NC Division of Air Quality, 1641 Mail Service Center, Raleigh, NC 27699-1641

Reisner, J., R. M. Rasmussen, and R. T. Bruintjes, 1998: Explicit forecasting of supercooled liquid water in winter storms using the MM5 mesoscale model. Quart. J. Roy. Metero. Soc., 124 B, 1071-1107.

Xiu, A., and J.E. Pleim, 2001: Development of a land surface model. Part I: Application in a mesoscale meteorology model. Journal of Applied Meteorology, 40, 192-209.

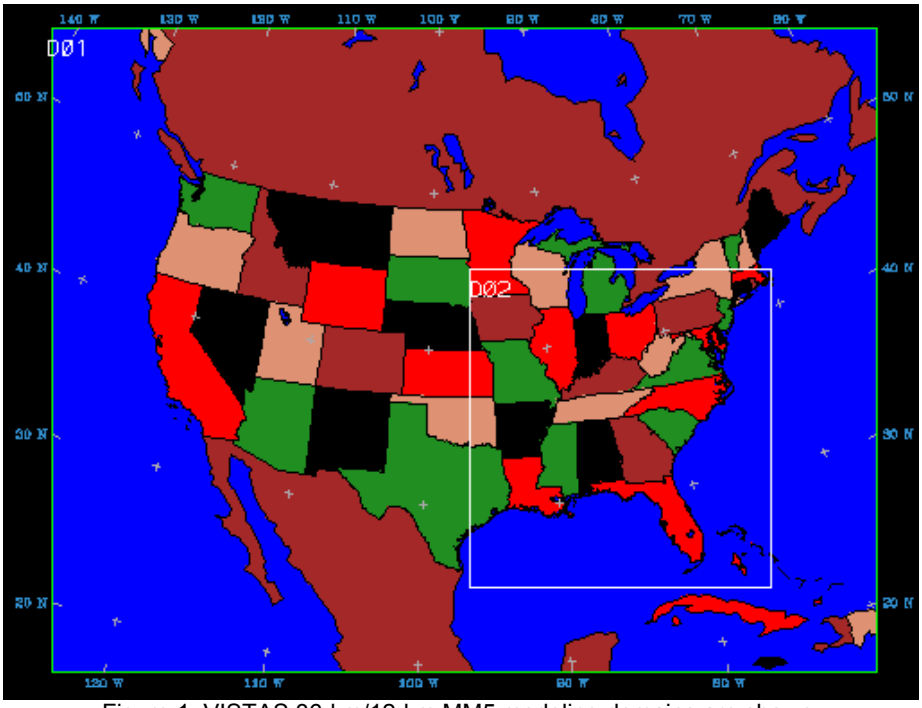

Figure 1. VISTAS 36-km/12-km MM5 modeling domains are shown.

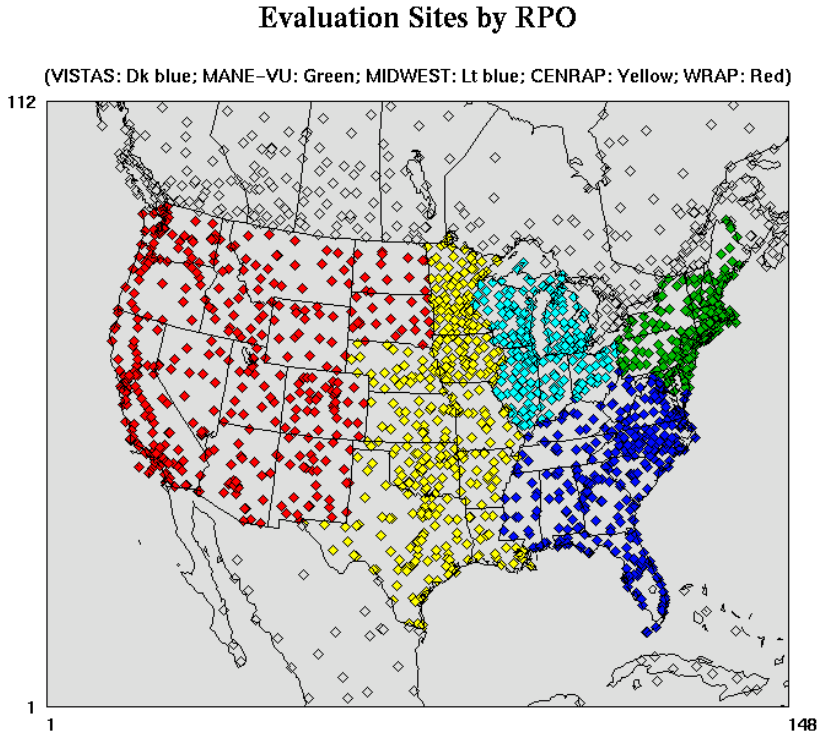

Figure 2. Surface observing network color-coded to represent Regional Planning Organization areas. Dark blue diamonds are in the VISTAS RPO, green diamonds are in the MANE-VU RPO, light blue diamonds are in the MIDWEST RPO, yellow diamonds are in the CENRAP RPO, and red diamonds are in the WRAP RPO. Gray diamonds represent sites out of the US portion of the modeling domain.

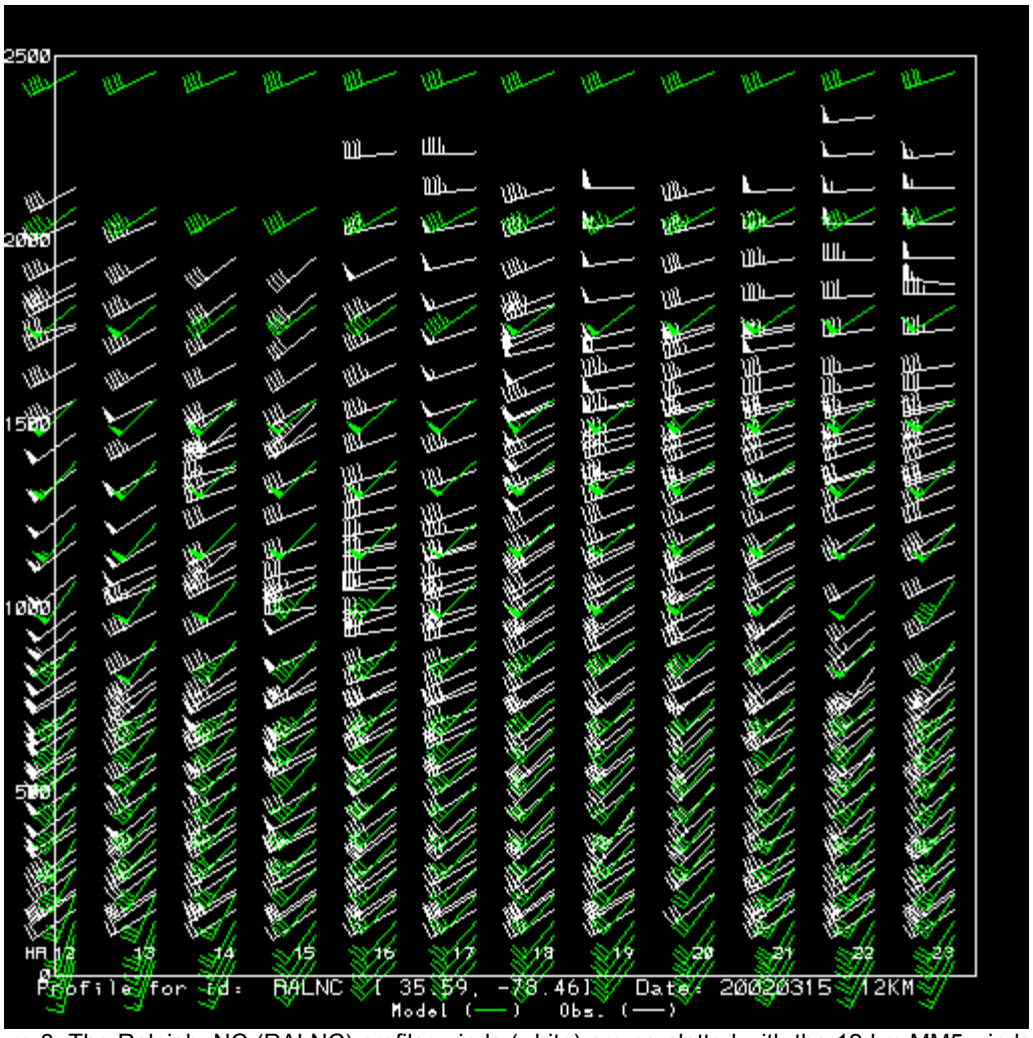

Figure 3. The Raleigh, NC (RALNC) profiler winds (white) are co-plotted with the 12-km MM5 winds (green) for 12-23 UTC on March 15, 2002.

Total_stats	obsmean	modmean	bias	abserr	r2	ia	rmse	nbias	jtot
TMP-1.5m_(K)	289.46	289.10	-0.36	1.87	0.859	0.951	2.37394	0.00116	30729
QV_(g/kg)	9.57	10.05	0.47	1.06	0.775	0.927	1.40093	-0.07477	30247
RH_(%)	80.80	86.26	5.46	9.42	0.530	0.813	12.98462	-0.09797	30246
WSPD-10m_(m/s)	2.93	3.23	0.29	1.29	0.410	0.767	1.62495	-99.00000	29488
SPD-lyr1_(m/s)	2.93	3.83	0.90	1.51	0.380	0.735	1.89940	-99.00000	29488
CLD_(%)	53.95	54.00	0.05	26.82	0.330	0.764	36.76081	-99.00000	29792
CLD2_(%)	53.95	58.22	4.28	26.36	0.307	0.760	39.19626	-99.00000	29792
TMP-lyr1_(K)	289.46	289.22	-0.24	1.87	0.854	0.949	2.39892	0.00074	30729

Wdir_stats	obsmean	modmean	bias	abserr	ubias	vbias	uerr	verr	newtot	dbias
WDIR_(deg)	190.87	183.85	-7.02	25.40	-0.089	0.314	1.15182	1.26613	29488	2.879

Table 1. Surface summary statistics are shown for the March 12-17, 2002 modeling segment for the 12-km VISTAS region.

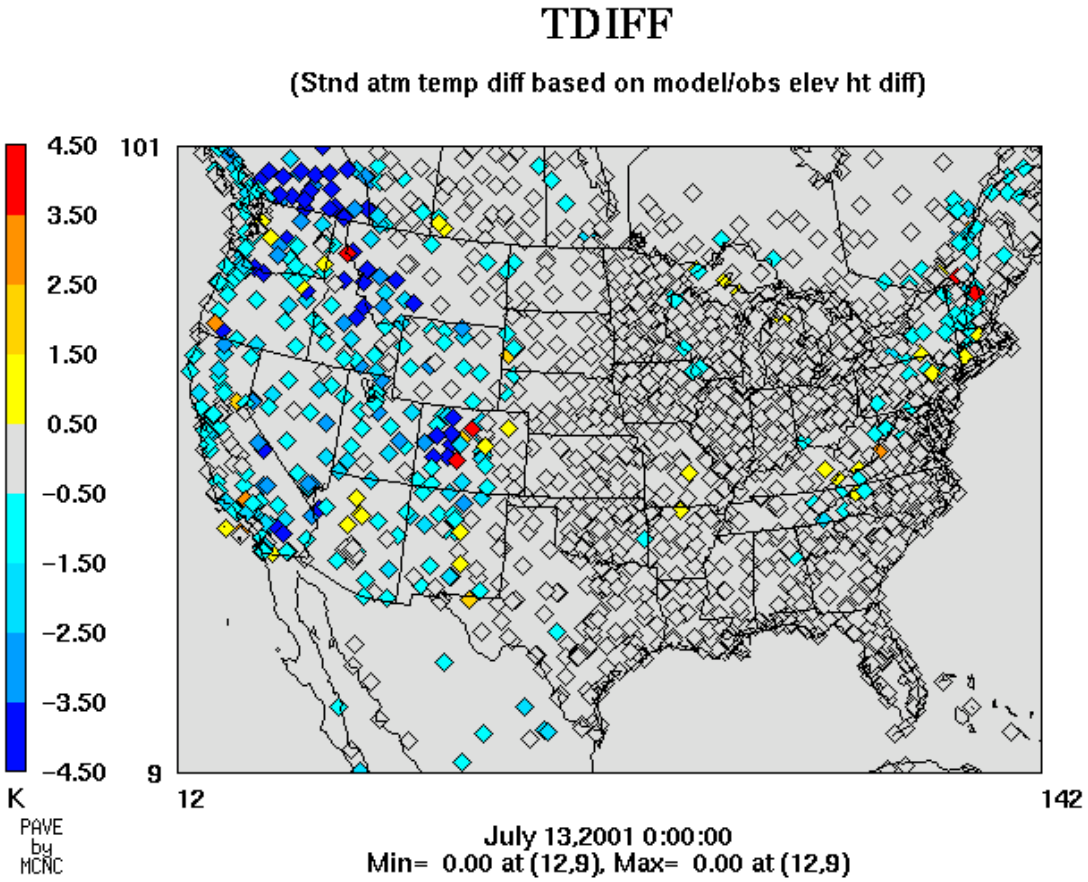

Figure 4. Model/obs elevation differences are converted to temperatures and plotted for the US portion of the 36-km grid. The temperatures are calculated assuming a standard atmosphere lapse rate of 6.5C/km, and practically indicate the temperature biases that might result solely by ignoring elevation-induced temperature effects. All of the observing sites are shown, including those sites that we ignore when calculating statistics due to their elevations being more than 500m different than the corresponding model elevations.

Total_stats	obsmean	modmean	bias	abserr	r2	ia	rmse	nbias	jtot
TMP-1.5m_(K)	277.89	276.87	-1.03	2.05	0.910	0.973	2.70059	0.00364	480126
QV_(g/kg)	4.46	4.63	0.17	0.58	0.936	0.983	0.83009	-0.06401	472271
RH_(%)	72.10	77.66	5.56	12.25	0.470	0.812	15.92663	-0.11393	472217
WSPD-regular_(m/s)	3.51	3.76	0.25	1.31	0.496	0.808	1.67567	-99.00000	466042
WSPD-nocalms_(m/s)	4.14	4.04	-0.10	1.14	0.444	0.805	1.50113	-0.08546	395406
WSPD-mincalm_(m/s)	3.63	3.76	0.13	1.19	0.502	0.823	1.54222	-0.35402	466042
SPD-lyr1_(m/s)	3.63	4.47	0.84	1.43	0.485	0.793	1.80626	-0.64790	466042
CLD_(%)	43.14	37.00	-6.14	24.52	0.414	0.792	35.41226	-99.00000	466016
CLD2_(%)	43.14	40.98	-2.15	23.30	0.411	0.805	35.95408	-99.00000	466016
TMP-lyr1_(K)	277.89	277.39	-0.50	1.97	0.906	0.974	2.58621	0.00173	480126

Wdir_stats	obsmean	modmean	bias	abserr	ubias	vbias	uerr	verr	newtot	dbias
WDIR_(deg)	255.83	254.29	-1.54	19.51	0.039	0.048	1.14482	1.21661	466042	1.667

Pcp threshold (in)	ACC	BIAS	THREAT	ETS	FAR	HK	HSS	POD	HITS	ZEROES	MISSES	FALSES
0.01	0.8665	1.0776	0.6672	0.5387	0.2285	0.7145	0.7002	0.8314	151526	338883	30719	44870
0.05	0.9187	1.0396	0.6962	0.6238	0.1948	0.7792	0.7684	0.8371	105380	414627	20501	25490
0.10	0.9342	1.0168	0.6881	0.6330	0.1915	0.7804	0.7753	0.8221	82119	446660	17770	19449
0.25	0.9555	0.9315	0.6602	0.6266	0.1754	0.7474	0.7705	0.7681	48901	491933	14764	10400
0.50	0.9665	0.9319	0.5626	0.5412	0.2536	0.6800	0.7023	0.6956	24395	522640	10676	8287
1.00	0.9851	0.8378	0.4887	0.4804	0.2799	0.5976	0.6490	0.6033	8042	549542	5288	3126

Table 2. January 2002 statistical table for the 12-km Full region is shown.

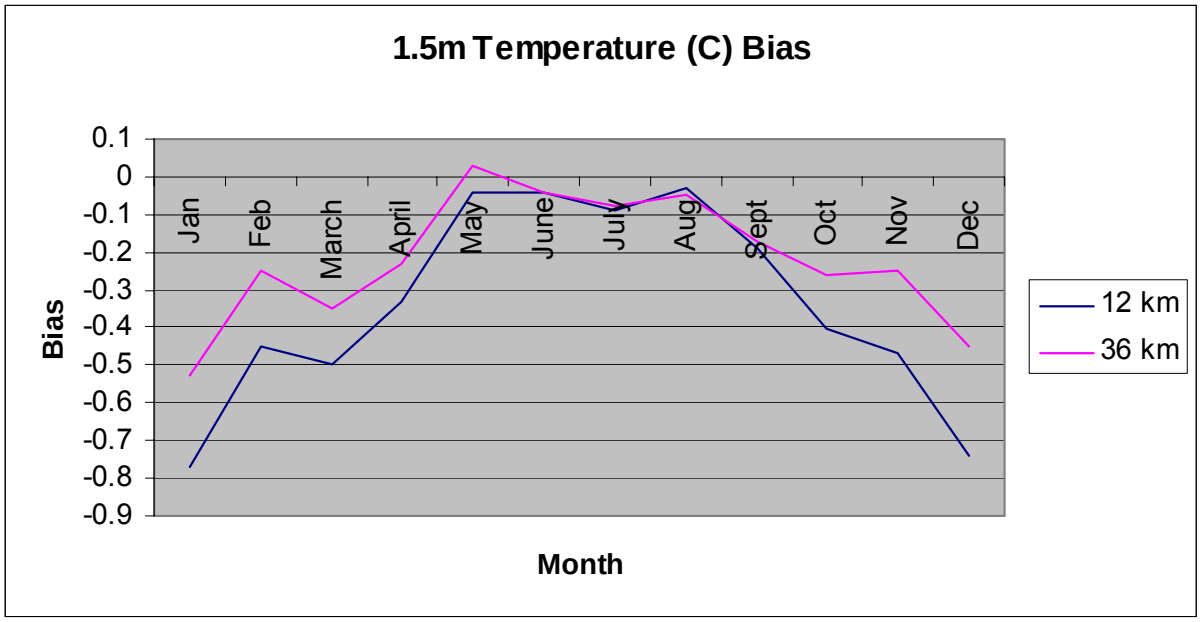

Figure 5. VISTAS region monthly temperature biases are plotted for both 12-km and 36-km resolutions.

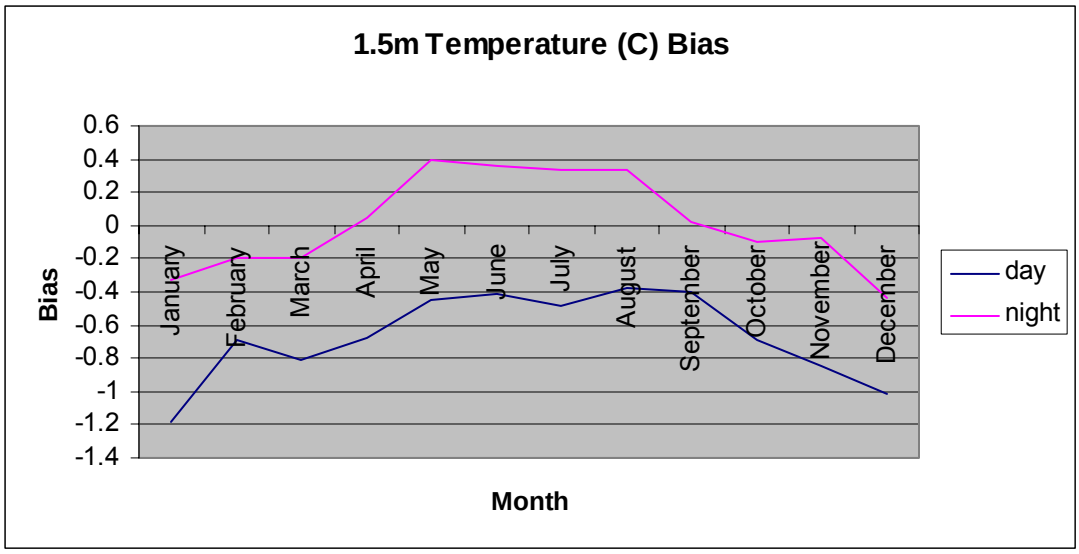

Figure 6. Monthly temperature biases for the 12-km VISTAS region are plotted. The "day" period is defined to be 12Z-23Z, while "night" is defined to be 00Z-11Z.

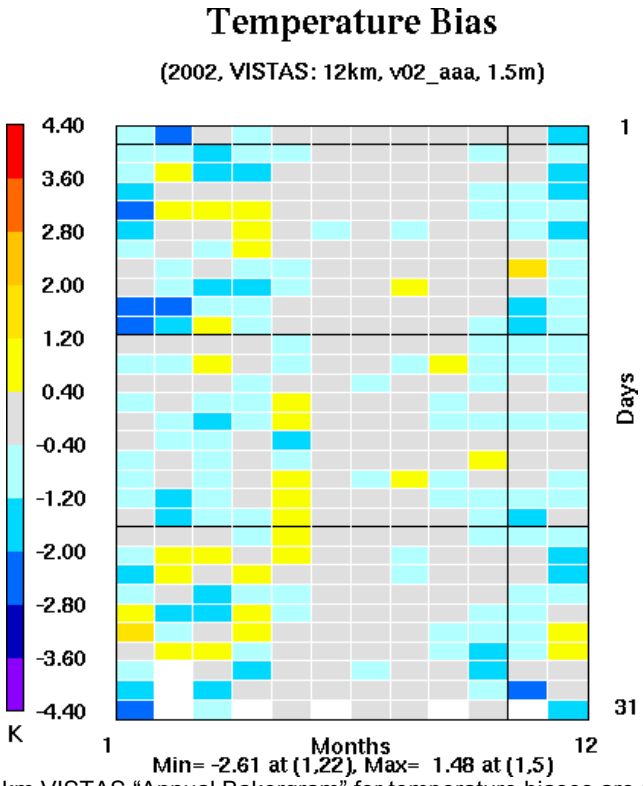

Figure 7. The 2002 12-km VISTAS "Annual Bakergram" for temperature biases are plotted. The data are shown in a calendar-like layout so that the upper left cell represents the bias on the first day of January.

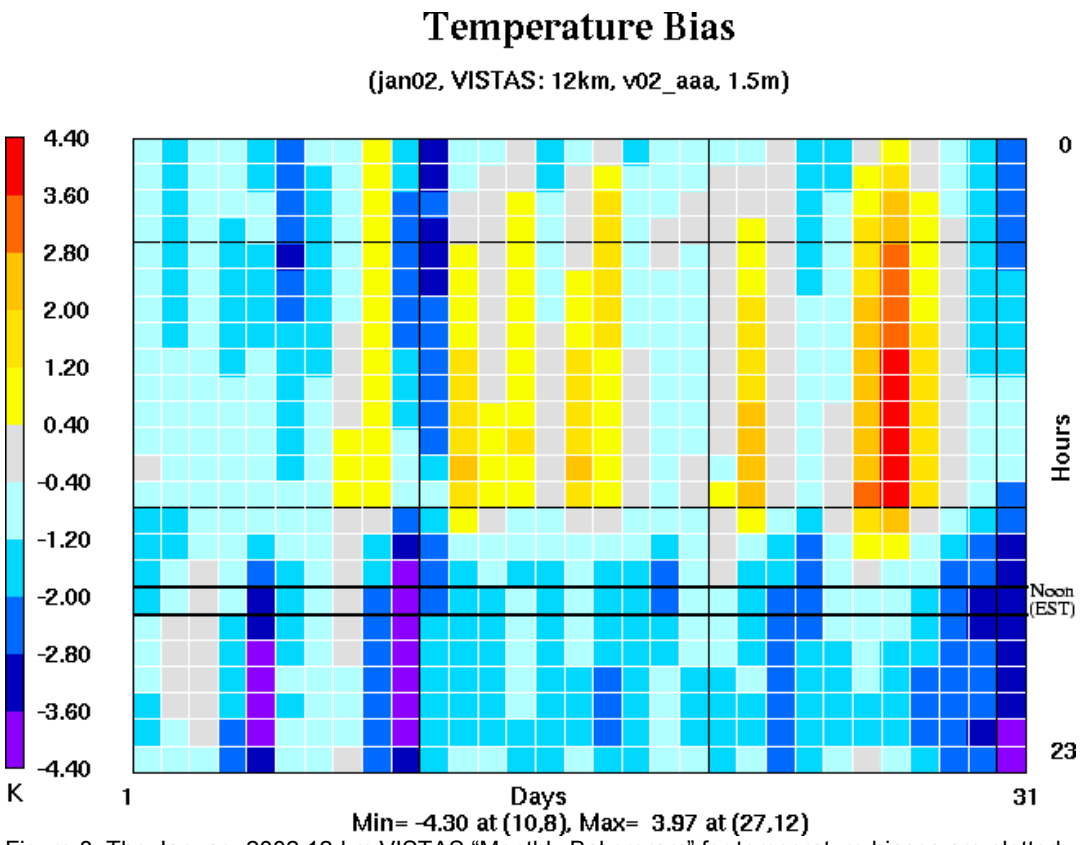

Figure 8. The January 2002 12-km VISTAS "Monthly Bakergram" for temperature biases are plotted. The hourly biases are shown in a calendar-like layout so that the upper left cell represents the 00Z bias on the first day of the month.

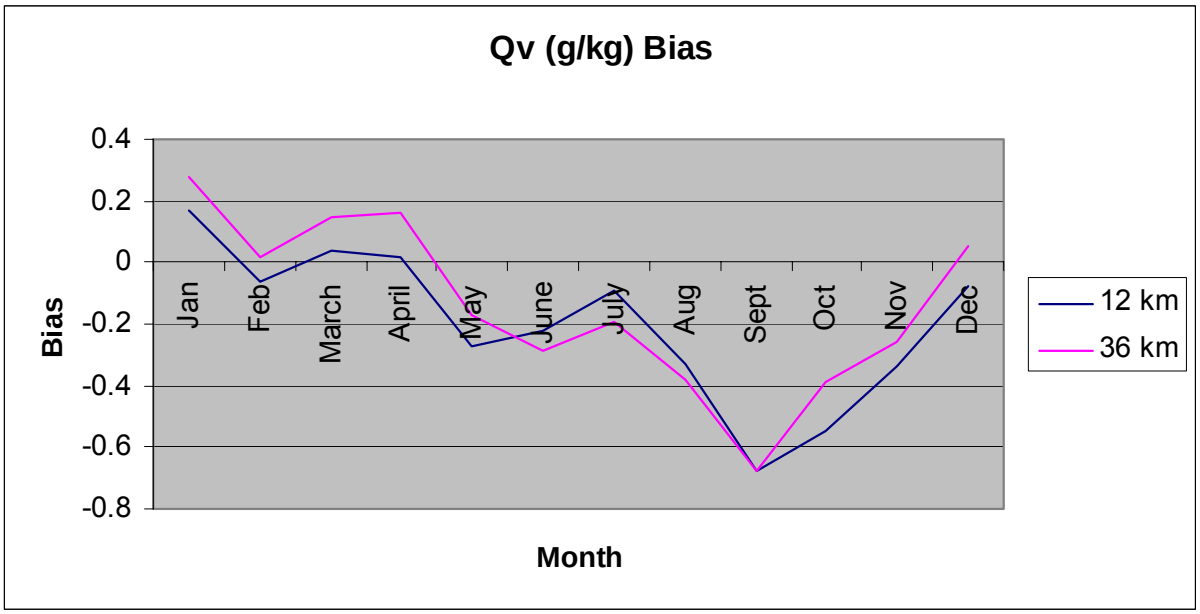

Figure 9. VISTAS region monthly mixing ratio biases are plotted for both 12-km and 36-km resolutions.

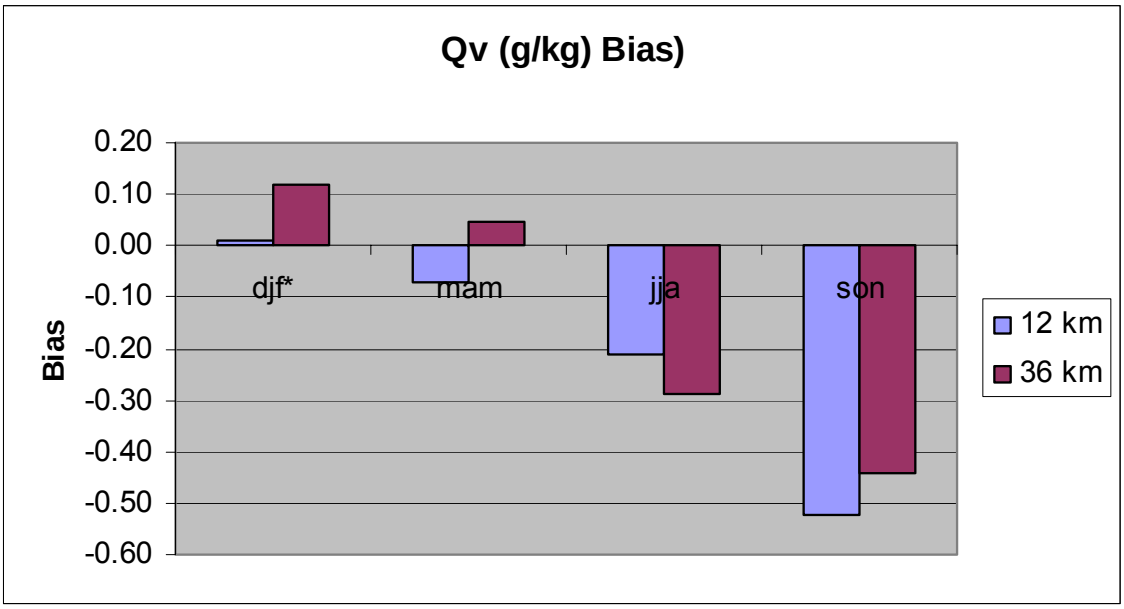

Figure 10. Seasonally aggregated VISTAS region mixing ratio biases are shown for both the 36-km and 12-km grids. *All months are in 2002, so the winter (djf) bar graph represents a discontinuous time period.

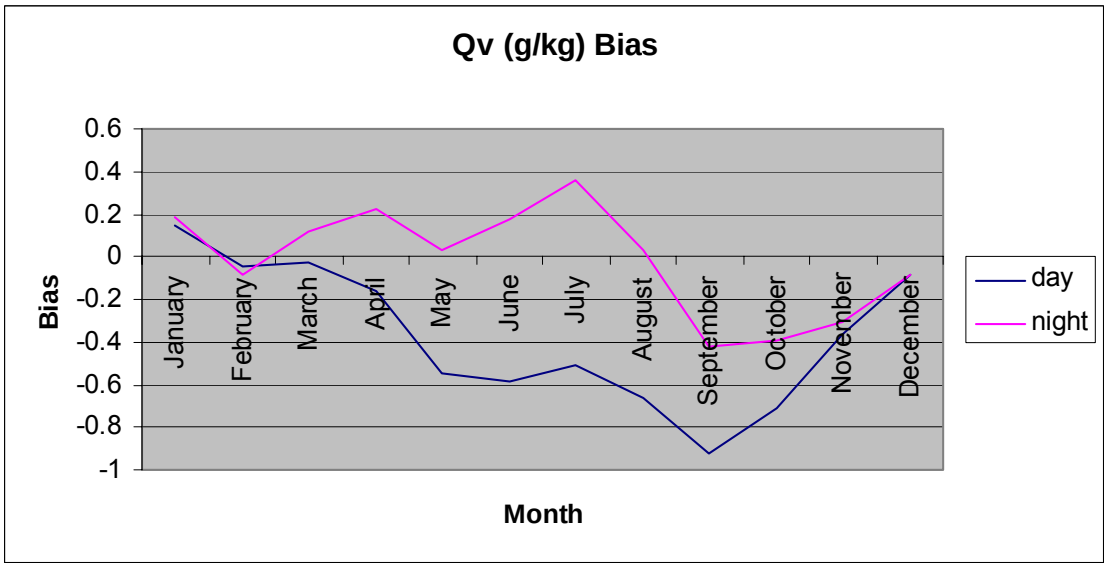

Figure 11. Monthly mixing ratio biases for the 12-km VISTAS region are plotted. The “day” period is defined to be 12Z-23Z, while “night” is defined to be 00Z-11Z.

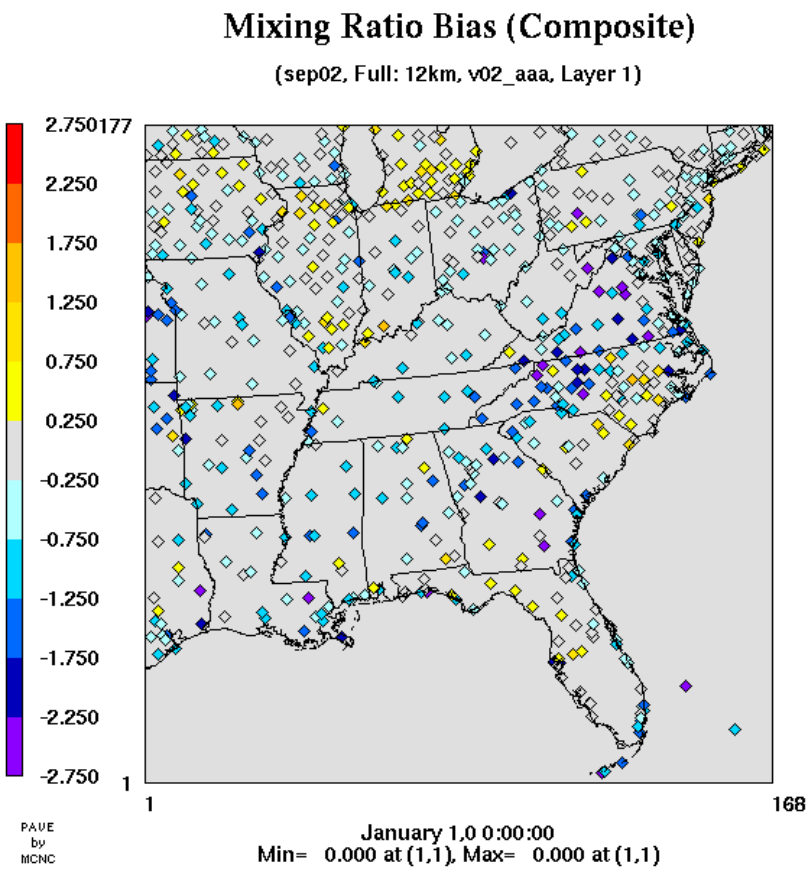

Figure 12. Site-specific mixing ratio biases (g/kg) for September 2002 are displayed for each site in the 12-km grid. Note that the PAVE date label (January 1, 0) is nonsensical and should be ignored since it is only a placeholder.

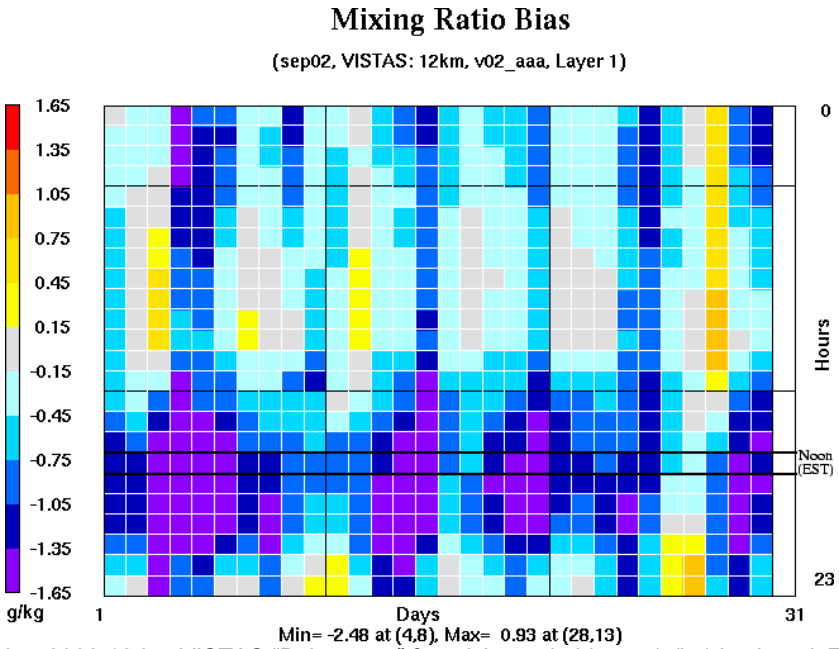

Figure 13. The September 2002 12-km VISTAS “Bakergram” for mixing ratio biases (g/kg) is plotted. The hourly biases are shown in a calendar-like layout so that the upper left cell represents the 00Z bias on the first day of the month.

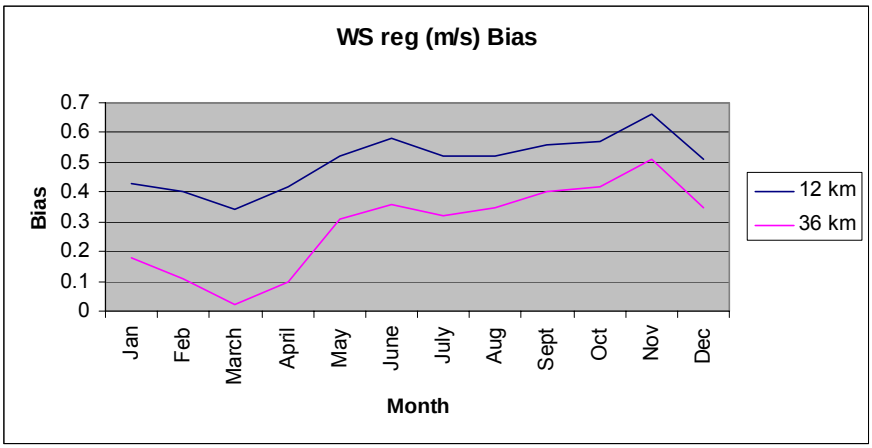

Figure 14. VISTAS region wind speed (regular) biases (m/s) are plotted for both 12-km and 36-km resolutions.

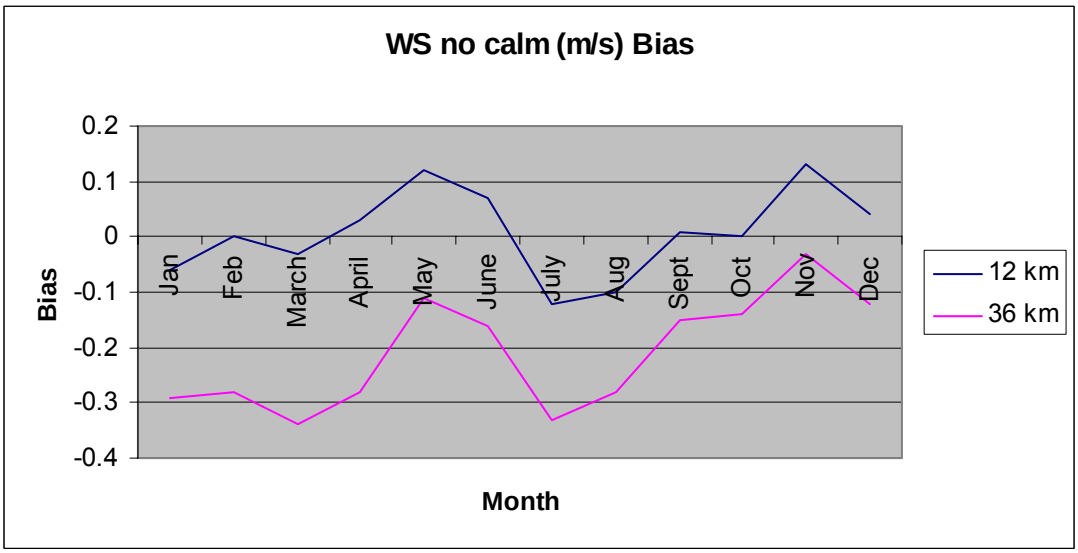

Figure 15. VISTAS region wind speed (no calms) biases (m/s) are plotted for both 12-km and 36-km resolutions.

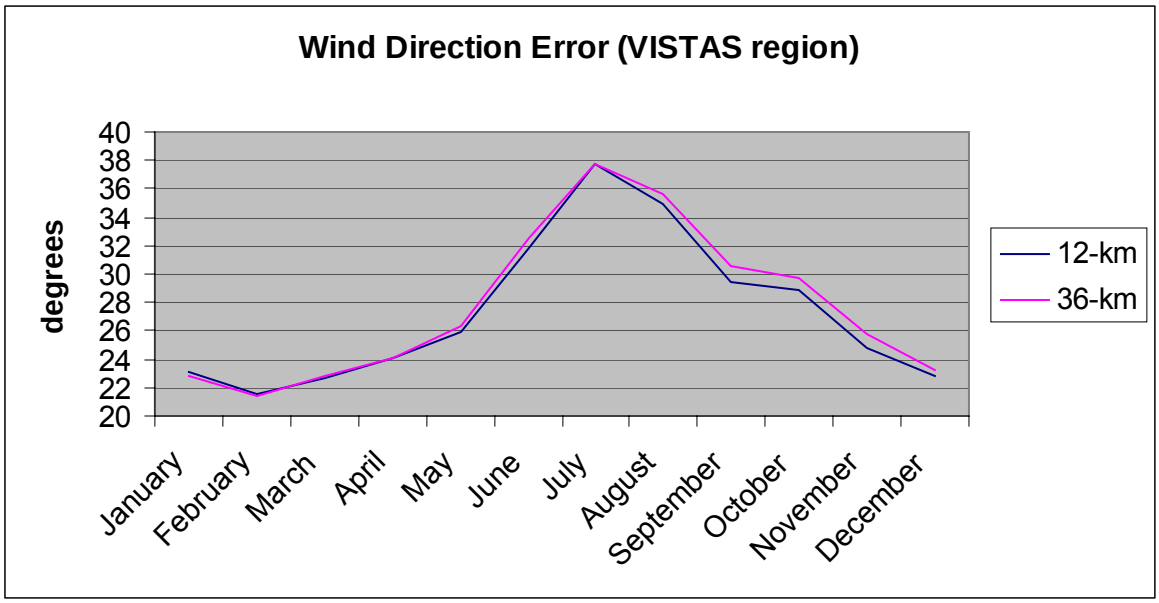

Figure 16. VISTAS region wind direction errors are plotted for both 12-km and 36-km resolutions.

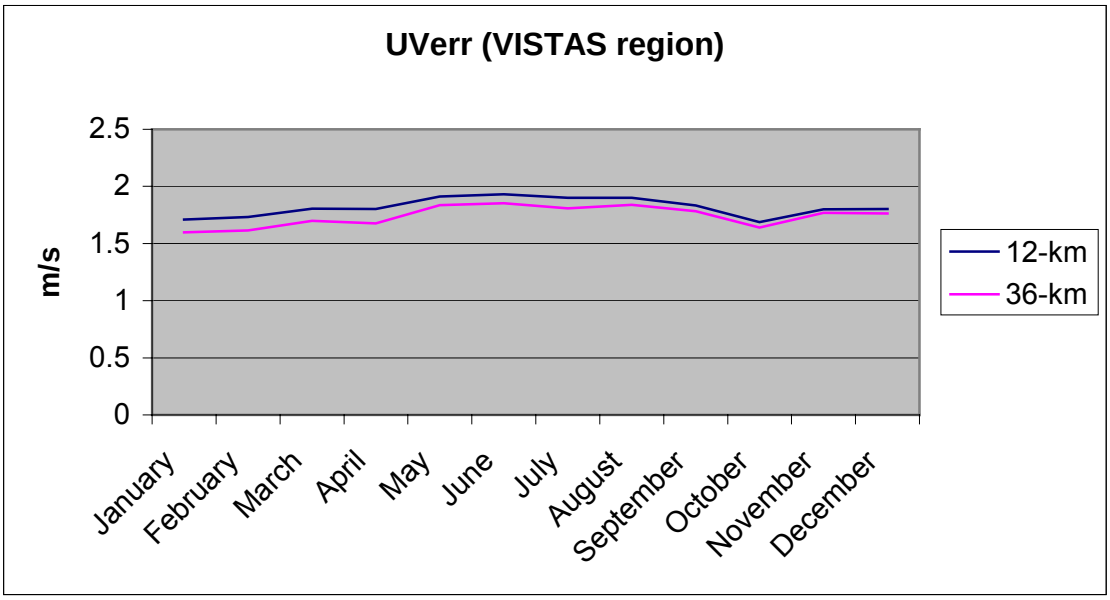

Figure 17. The magnitude of the error wind vector for the VISTAS region is plotted for both 12-km and 36-km resolutions.

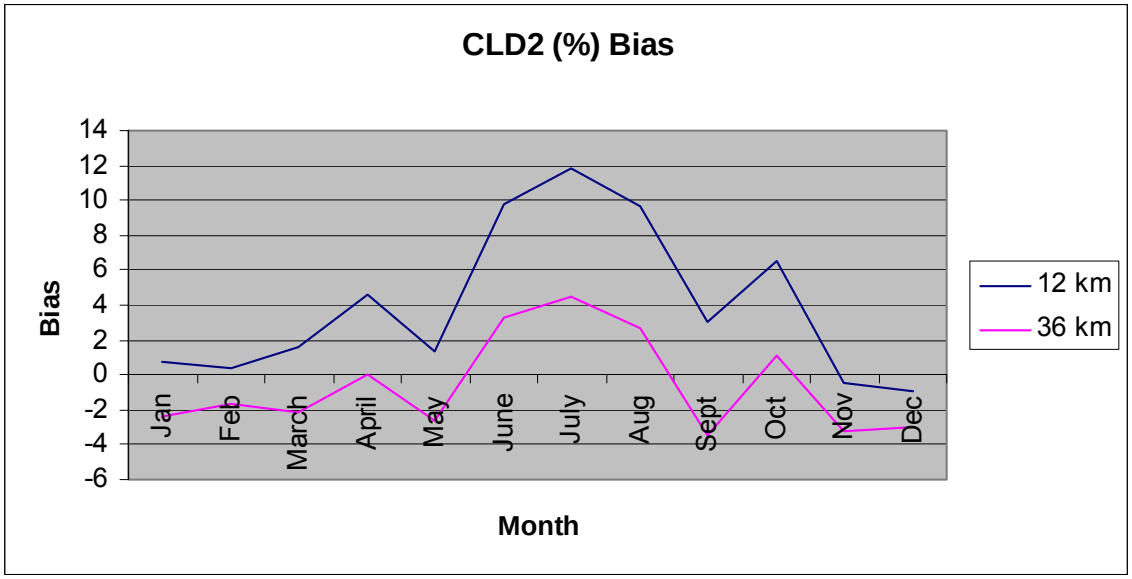

Figure 18. VISTAS region alternative cloud biases are plotted for both 12-km and 36-km resolutions.

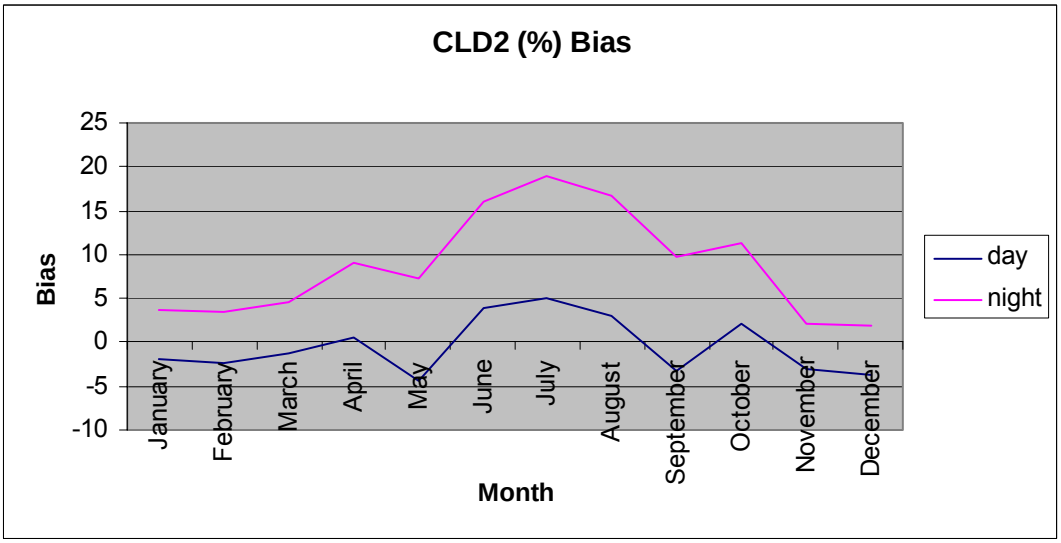

Figure 19. Monthly alternative cloud biases for the 12-km VISTAS region are plotted. The “day” period is defined to be 12Z-23Z, while “night” is defined to be 00Z-11Z.

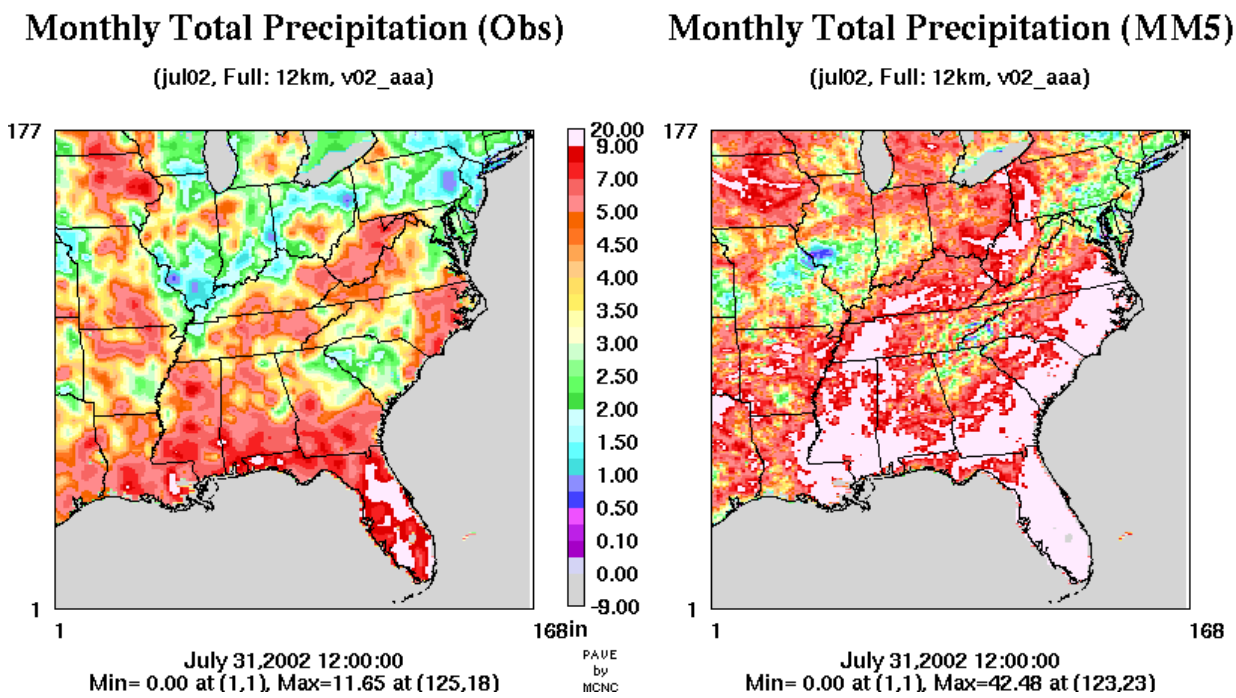

Figure 20. The July 2002 12-km accumulated precipitation from the Climate Prediction Center is juxtaposed with the MM5 accumulated precipitation.